Thin-Walled Structures 139 (2019) 66–76

Contents lists available at ScienceDirect

Thin-Walled Structures

journal homepage: www.elsevier.com/locate/tws

Full length article

Behavior of axially loaded circular stainless steel tube confined concrete stub columns

Lanhui Guo[a,*], Yong Liu[a], Feng Fu[b], Haijia Huang[a]

[a] School of Civil Engineering, Harbin Institute of Technology, Harbin, China
[b] School of Mathematics, Computer Science & Engineering, City, University of London, EC1V 0HB, UK

ARTICLE INFO

Keywords:
Stainless steel tube
Steel tube confined concrete
Stub columns
Axially loaded
Experimental study

ABSTRACT

Stainless steel tube confined concrete (SSTCC) stub column is a new form of steel-concrete composite column in which the stainless steel tube is used to confine the core concrete without resistance to the axial load directly. It could take the advantages of both the stainless steel tube and the steel tube confined concrete columns. This paper presents the experimental investigation of circular SSTCC stub columns subjected to axial load. Meanwhile, comparative tests of the circular concrete-filled stainless steel tubes and circular hollow stainless steel tubes were also conducted. The experimental phenomena of specimens are introduced in detail and the experimental results are analyzed. Through the investigation of axial stress and hoop stress on the stainless steel tube, the interaction between stainless steel tube and core concrete is studied. The experimental results showed that the stainless steel tube provides confinement to the core concrete, increasing the compressive capacity of core concrete significantly. In addition, the confinement of stainless steel tube in SSTCC stub columns is larger than that in concrete-filled stainless steel tubes. Therefore, the load-carrying capacity of SSTCC columns is higher than that of concrete-filled stainless steel tubes. Besides, an equation was proposed to calculate the load-carrying capacities of SSTCC columns and concrete-filled stainless steel tube columns. The calculated results agree well with the experimental results.

1. Introduction

The conventional carbon steel tube confined concrete columns is a type of steel-concrete composite column, in which the steel tube is discontinuous at the beam-column joints [1–3]. As shown in Fig. 1, the steel tube is cut at both ends close to beam-column connection in steel tube confined concrete members, comparing with concrete-filled steel tube columns. Thus, the steel tube would not resist the vertical load directly, and its confinement to the core concrete is better than that in concrete-filled steel tubes. Besides this, for steel tube confined concrete columns, the beam-column connection make it easy for the construction of rebar and pouring concrete if the reinforced concrete beam is applied. Meanwhile, the steel tube can act as the formwork during the construction stage, making it easier to cast the concrete. Besides, sufficient researches [4–11] have been conducted on the behaviors of the steel tube confined concrete columns, which indicates that such type of members has relatively high bearing capacity, good ductility as well as excellent fire resistance. Due to the excellent mechanical and manufacture properties, steel tube confined concrete columns are used increasingly in projects, especially in the Middle East and the East Asia region.

Compared with carbon steel, stainless steel possesses natural corrosion resistance. Thus, after being appropriately processed, the surface can be exposed to natural environment without any extra protective coatings. Besides, stainless steel also exhibits features, such as the ease of maintenance, ease of construction and high fire resistance compared with traditional carbon steel. Therefore, stainless steel tube could be used in the steel tube confined concrete column, which is stainless steel tube confined concrete (SSTCC) columns. Apart from the above mentioned advantageous of steel tube confined concrete columns, the stainless steel tube confined concrete columns also have the fine aesthetic appearance and high corrosion resistance benefiting from the material of stainless steel. Although the initial cost is higher using stainless steel tube, the overall cost may overcome this shortage considering the life-cycle cost and maintenance of the conventional carbon steel tube columns.

In the past, experimental and theoretical studies [4–11] had been conducted on the behaviors of carbon steel tube confined concrete columns, which included behavior under axial load, eccentric load and seismic load. Both the square and circular shape cross-sections were

* Corresponding author.
E-mail address: guolanhui@hit.edu.cn (L. Guo).

https://doi.org/10.1016/j.tws.2019.02.014
Received 8 October 2018; Received in revised form 5 January 2019; Accepted 13 February 2019
Available online 05 March 2019
0263-8231/

Notations

A_c	Cross-sectional area of concrete core
A_s	Cross-sectional area of stainless steel tube
D	Out-diameter of stainless steel tube
E_s	Elastic modulus of stainless steel
E_s^t	Tangent modulus on the plastic stage of stainless steel
f_{cu}^{100}	Compressive strengths of 100 mm concrete cubes
f_{ck}	Compressive strengths of 150 mm concrete cubes
f_r'	Effective confining stress of circular tube on the concrete
f_p	Proportional yield strength of stainless steel
N_s	Axial force on stainless steel tube
N_c	Axial force resisted by core concrete
N_{ue}	Ultimate compressive strength of specimen
t	Thickness of stainless steel tube
$\sigma_{0.2}$	Yield strength in accordance to 0.2% of plastic strain for stainless steel
σ_h	Hoop stress on stainless steel tube
σ_v	Vertical stress on stainless steel tube
σ_z	Equivalent stress on stainless steel tube
ε_h	Hoop strain on stainless steel tube
ε_v	Vertical strain on stainless steel tube
μ_s	Poisson's ratio of stainless steel
μ_{sp}	Poisson's ratio for the stainless steel in the plastic stage

studied. Based on these studies, the methods to calculate load-carrying capacities of carbon steel tube confined concrete columns were proposed [12–14].

Compared with the carbon steel, stainless steel generally has a stress–strain curve with no yield plateau and follows different stress–-strain curve under tension and compression. Besides, the ductility of stainless steel is much better than that of carbon steel. Because of the different properties of stainless steel, some researchers such as Young and Ellobody [15–17] studied the behavior of concrete-filled stainless steel tube (CFSST) columns. A series of tests were conducted to investigate the effects of the shape of stainless steel tube, plate thickness and concrete strength on the behavior and strength of axially loaded CFSST columns. Lam and Gardner [18] tested eight CFSST columns and eight concrete-filled carbon steel tube columns with square section. They also compared the strengths of those members with those determined by the existing design methods for composite carbon steel sections in Eurocode 4 and ACI 318. In addition, a new method to predict the axial capacity of concrete-filled stainless steel hollow sections was also developed. In 2013, Hassanein et al. [19] performed finite element analysis on the behavior of CFSST columns. Abdalla et al. [20] tested thirty-five concrete-filled stainless steel tube columns to investigate the effect of different parameters on their behavior. Two concrete compressive strengths of 44 MPa and 60 MPa and three diameter-to-thickness ratios of 54, 32, and 20 were considered. The axially loaded behavior of concrete-filled stainless/carbon steel double skin columns was studied by Ye et al. [21], Han et al. [22] and Wang et al. [23]. Chen et al. [24–27] did a series of research works on the behavior of CFSST columns, which includes the bond behavior between tube and concrete and the flexural behavior of the members. Li et al. [28] tested the concrete-filled stainless steel tube stub columns and double-skin stainless tube stub columns under axial compression, and the concrete was made of seawater and sea sand. A fiber element model incorporating the full-range three-stage stress–strain relationships was developed by Patel et al. [29] for the nonlinear analysis of CFSST short columns under axial compression. This model could accounts for the concrete confinement effects provided by the stainless steel tube. Dabaon et al. [30] performed finite element analysis and compared the confinement effect of stiffened and unstiffened concrete-filled stainless steel tubular stub columns.

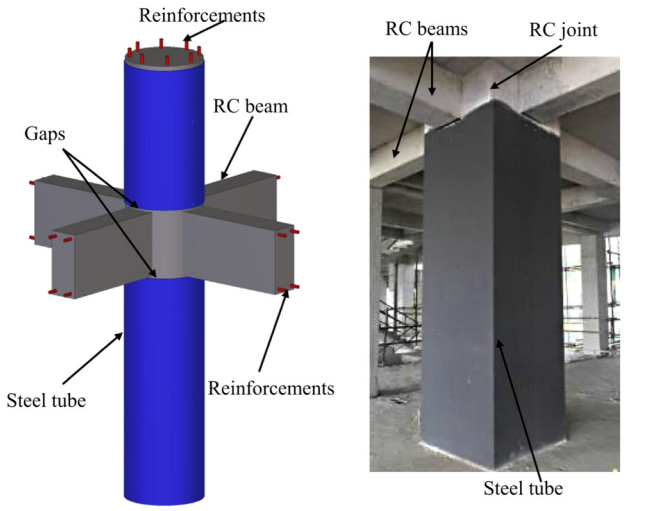

Fig. 1. Steel tube confined concrete columns.

The above literature review indicates that past studies were mainly focused on carbon steel tube confined concrete columns or concrete-filled stainless steel tube columns. Currently, little research has been conducted on SSTCC columns. To understand the behavior of SSTCC columns clearly, a series of tests were conducted under axial compression. For comparison purposes, concrete-filled stainless steel tubular columns and hollow stainless steel tubes were also tested. At last, an equation to calculate the load-carrying capacity of SSTCC columns subjected to axial load was suggested.

2. Experimental study

2.1. Test specimens

In order to understand the behaviors of stainless steel tube confined concrete (SSTCC) columns, 18 specimens were tested under monotonic loaded axial compression using the 5000 kN capacity high-stiffness compression machine at the structural lab in Harbin Institute of Technology. Among these 18 specimens, nine are stainless steel tube confined concrete stub columns, six specimens are concrete-filled stainless steel tube stub columns, and three specimens are hollow stainless steel tubes columns. All specimens are stub columns with a height-to-diameter ratio of 3.0 to eliminate the end effect and column slenderness effect. The dimensions of all specimens are presented in Fig. 2 and Table 1. Two kinds of thicknesses of steel plates are selected, which are 1.3 mm and 1.65 mm. The diameter-to-thickness ratio varies from 89 to 109.

All the employed tubes were produced by rolling the steel plate to circular members, and then weld the steel tube by a butt weld. A rigid end plate with 10 mm thickness was welded to the bottom of the tube. The concrete was filled into the tube and after 28 days of curing, another rigid steel plate was covered and welded to the top of the tube. The surface of end plates was smooth and flat after grinding using a grinder with diamond cutters. This was to ensure that the load was applied evenly across the cross-section and simultaneously to the steel tube and the core concrete. To ensure the axial load is applied only to the core concrete in SSTCC columns, two 10 mm wide girth strips were cut off from the steel tube at 30 mm away from the end plates, as shown in Fig. 2.

(a) Concrete-filled stainless steel tube columns (b) Stainless steel tube confined concrete members

Fig. 2. Dimension of the specimen.

Table 1
Geometric and material properties of specimens.

Specimens	H/mm	D/mm	t/mm	D/t	$\sigma_{0.2}$/MPa	f_c'/MPa
SSTCC-D125-a	374.5	125.3	1.29	97	496	54.5
SSTCC-D125-b	374.9	124.8	1.25	100	496	54.5
SSTCC-D125-c	374.8	124.5	1.33	94	496	54.5
CFSST-D125-a	375.3	124.8	1.31	95	496	54.5
CFSST-D125-b	374.5	125.3	1.30	96	496	54.5
SST-D125-a	375.5	124.8	1.31	96	496	–
SSTCC-D150-a	444.9	149.7	1.63	92	493	54.5
SSTCC-D150-b	444.8	149.8	1.67	90	493	54.5
SSTCC-D150-c	445.1	150.2	1.67	90	493	54.5
CFSST-D150-a	444.8	150.1	1.68	89	493	54.5
CFSST-D150-b	444.9	149.8	1.65	91	493	54.5
SST-D150-a	445.0	150.2	1.66	90	493	–
SSTCC-D180-a	540.4	180.8	1.68	108	493	54.5
SSTCC-D180-b	540.5	180.6	1.65	109	493	54.5
SSTCC-D180-c	539.8	180.7	1.67	108	493	54.5
CFSST-D180-a	539.7	180.7	1.69	107	493	54.5
CFSST-D180-b	540.4	180.7	1.70	106	493	54.5
SST-D180-a	539.9	180.8	1.70	106	493	–

Note: In the nomenclature of the group, 'SSTCC' is the abbreviation of circular stainless steel tube confined concrete; 'CFSST' is the abbreviation of circular concrete-filled stainless steel tubes; 'SST' is the abbreviation of circular hollow section stainless steel tubes. "D125" means the nominal diameter of the specimen is 125 mm while "a" is the number for the specimen of the same type.

2.2. Material properties

The stainless steel employed in the specimen is the austenitic stainless steel section of ASTM (American Standard for Testing and Materials) 304. In order to determine the property of stainless steel, three tensile coupons were cut from a random location of the selected steel sheet. The coupons were made and tested in accordance with the Chinese standard GB/T 228-2002 [31]. The typical tensile stress–strain curve of stainless steel is presented in Fig. 3. As can be seen, the stress–strain curve of the stainless steel has no yield plateau but good ductility. For steel plates with the thickness of 1.3 mm and 1.65 mm, the elastic moduli of steel plates are 217 GPa and 215 GPa, and the average yield strengths are 496 MPa and 493 MPa, respectively. The ultimate strength of steel plates with the thickness of 1.3 mm and 1.65 mm are 777 MPa and 780 MPa, respectively.

When casting concrete, three concrete prisms with the dimension of 150 mm × 150 mm × 300 mm were casted and cured in the same conditions as the specimens. The test procedure was in accordance with the Chinese standard GB/T 50081-2002 [32]. The average compressive strength of concrete is 54.5 MPa. The average modulus of concrete is 38,100 MPa.

2.3. Experimental setup and load schedule

As shown in Figs. 4 and 5, eight strain gauges were glued to the mid-height of the specimen, which were arranged in the longitudinal and transverse directions with 90° angles. Four displacement transducers were used to measure the axial deformation. Fig. 4 illustrates the experimental setup.

The tests were conducted using a 5000 kN capacity universal testing machine in Harbin Institute of Technology, and the load was applied directly on the specimen. The tests were firstly loaded with a controlled increment of the rate of 0.06 MPa/s. When the yielding of specimen started (the maximum strain reached the yielding strain of steel plate), the loading process turned into the displacement control with the rate of 10 με/s. The tests were terminated when the axial load decreased to 75% of the peak load caused by the fracture of steel plate or crushing of concrete.

3. Experimental phenomena

3.1. Stainless steel tube confined concrete stub columns

During the initial loading stage, no significant changes were observed. Before the axial load reached 80% of peak load, the relationship between axial load and deformation was kept as linear, and the specimen was in the elastic stage. After the load exceeded 80% of peak load, the axial displacement started to increase quickly with the increase of axial load. When the axial load reached 98% of peak load, small cracking appeared at the position of cutting of steel tube. When the specimen reached the peak load, the concrete at the cutting position

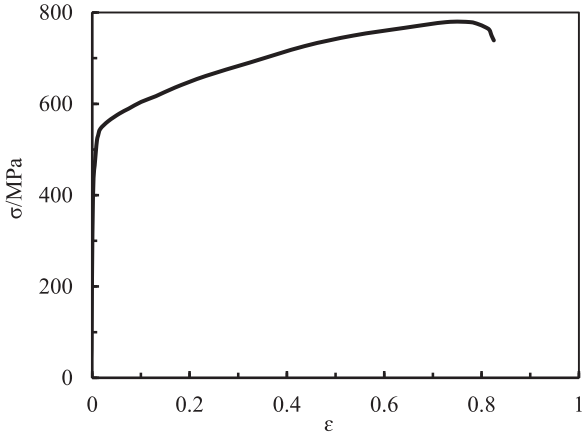

Fig. 3. Stress–strain relationship of stainless steel with thickness of 1.3 mm.

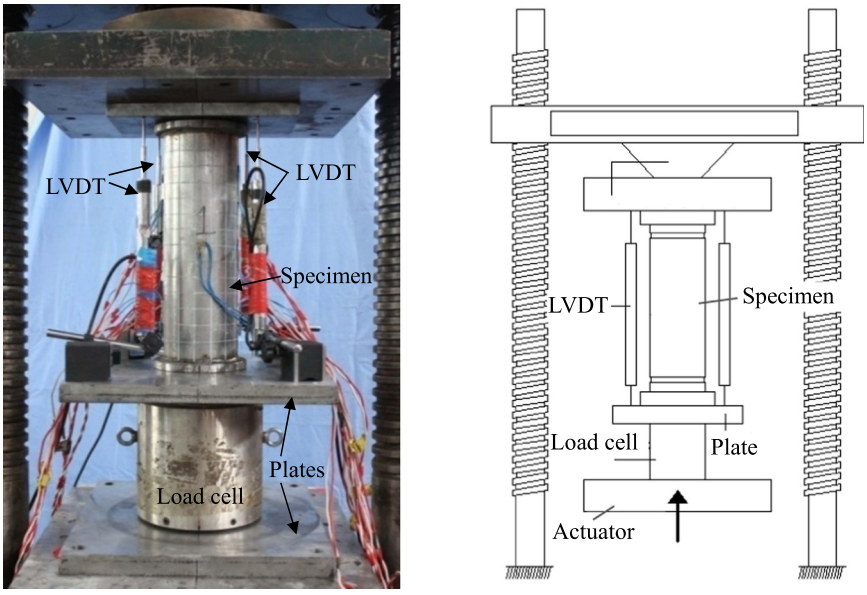

(a) Photo of test setup (b) Diagram of setup

Fig. 4. Experimental setup.

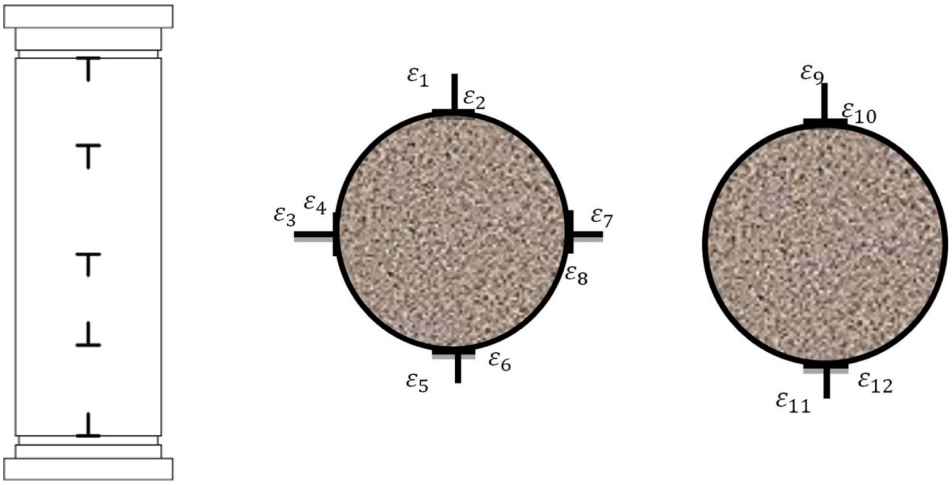

(a) Side view of columns (b) Section at mid-height (c) End and quartile section

Fig. 5. Location of strain gauges.

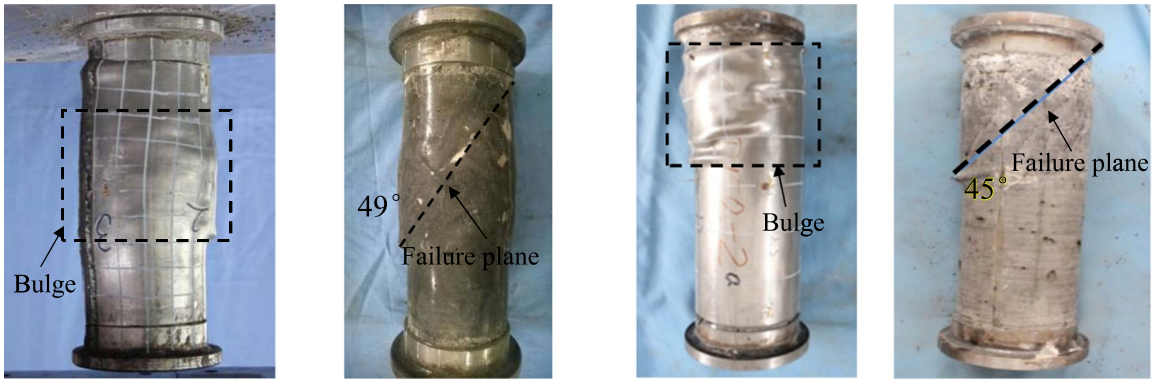

(a) Phenomena of specimen SSTCC-D125-a (b) Phenomena of specimen SSTCC-D150-b

Fig. 6. Failure mode of stainless steel tube confined concrete members.

of steel tube spalled. Then the axial load decreased slowly with the increase of axial deformation. When the axial load decreased to 85% of peak load, the lateral deflection of steel tube was observed, and the steel tube was slightly bloated without significant local buckling. To observe the damage of core concrete, the steel tubes were cut off and removed after the test. It was noticed that the core concrete failed in a shear failure mode with severe cracks along the diagonal direction. The angle between shear failure plane and the horizontal direction was about 45°~49°. The experimental phenomena of typical specimens are shown in Fig. 6. For specimens with a diameter of 150 mm, when the axial load decreased to 93% of the peak load, the steel tube at the position of welding broke, thus the load started to decrease sharply. The reason was that the steel tube cannot provide confinement to the core concrete anymore. Therefore, it is noticeable that, the quality of longitudinal weld is essential for this type of structural members, especially for the sake of sufficient ductility of the specimen.

3.2. Concrete-filled stainless steel tubular columns

For concrete-filled stainless steel tubular columns, the phenomena of all specimens were similar to each other. Taking specimen CFSST-D125-b as an example, the phenomena and failure mode were introduced in the following. Before the axial load reached 80% of peak load, there was no evident phenomenon on the surface of the specimen. The relationship between axial load and vertical deformation kept linear. When the specimen reached 80% of peak load, the stiffness of axial load-deformation relationship curve began to decrease. The local bulge of steel tube was observed near the bottom (about 50 mm from end plate). The bulge gradually increased with the increase of vertical deformation. The peak load of the specimen was 1142 kN and the corresponding vertical displacement was 2.72 mm. When the axial load decreased to 95% of peak load, the steel tube bloated at the mid-height position. When the axial load decreased to 90% of peak load, the axial load decreased very slowly with the increase of vertical deformation. The specimen exhibited global shear failure mode. The angle between the shear failure plane and horizontal plane was located between 48°~53°. The experimental phenomena were shown in Fig. 7.

3.3. Hollow stainless steel tubes with circular section

According to the Eurocode 3 'Design of Steel Structures, Part 1–4: General rules-Supplementary rules for stainless steels', if the diameter-to-thickness ratio (D/t) of stainless steel tube exceeds the limitation in Eq. (1), the local buckling would be trigged for circular hollow stainless steel sections before the steel reaches its yield strength.

$$\frac{D}{t} = 90\frac{235}{\sigma_{0.2}}\frac{E_s}{210000} \quad (1)$$

According to the Chinese Technical specification for stainless steel structures, if the diameter to thickness ratio is over $100*235/\sigma_{0.2}$, the local buckling of circular hollow section stainless steel stub would be considered. Considering the yield strength of stainless steel of 493 MPa, the limit diameter-to-thickness ratios for local buckling are 42.9 and 47.7 according to EC 3 code and Chinese design code, respectively. In the test, for specimens with the diameter of 125 mm, 150 mm and 180 mm, the corresponding diameter-to-thickness ratios are 96, 90 and 106, respectively. It can be seen that the circular stainless steel tube would fail in the elastic stage.

For specimens with hollow stainless steel section, there is no evident change at the initial loading stage. The axial load-deformation relationship kept linear before the axial load reached 80% of their bearing capacities. Beyond this, the deformation increased significantly with the increase of axial load. The rigidity of axial load-deformation relationship curve began to decrease. When the axial load reached the peak load, the inward local buckling near the bottom occurred accompanied by a sudden drop of the axial load and the increase of vertical displacement. The reason was that the specimen failed at the elastic stage of steel. From these specimens, it can be seen that severe buckling ripples appeared on the steel tubes. The experimental phenomena are shown in Fig. 8. When the load dropped to 50% of peak load, the vertical deformation reached the 1/50 of the specimen height. The test was terminated.

4. Experimental results analysis

4.1. Interaction behavior between steel tube and core concrete

4.1.1. Stress–strain relationship of stainless steel under biaxial stresses

In 2008, Quach et al. [33] developed a three-stage stress–strain relationship that is based on the extensive theoretical and experimental research works. In this paper, the authors further modified the formula based on the regression of the test results of stainless steel coupons presented in this paper. The modified formulae agree well with the stress–strain relationship of stainless steel. The formulae are as follows:

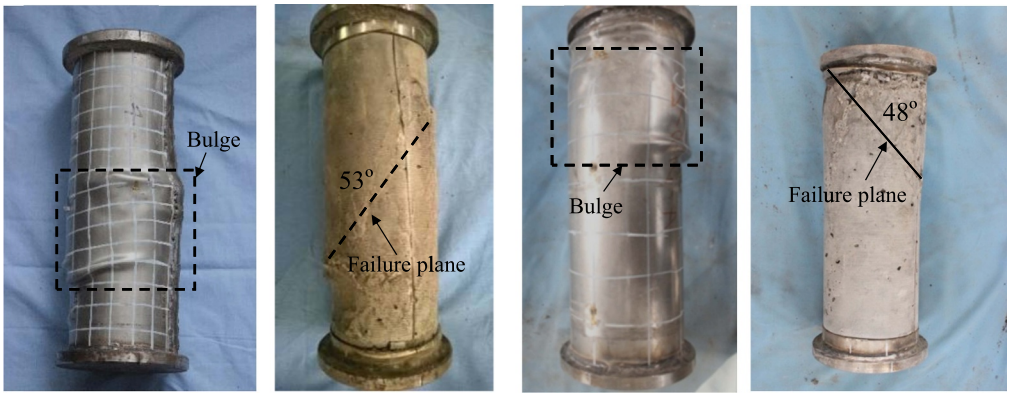

(a) Phenomena of specimen CFSST-D125-a (b) Phenomena of specimen CFSST-D150-b

Fig. 7. Failure mode of concrete-filled stainless steel tubes.

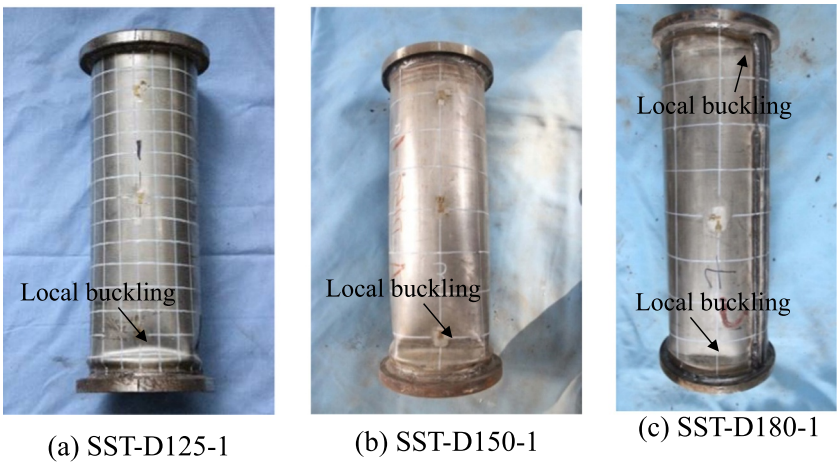

Fig. 8. Experimental phenomena of stainless steel tubes with circular hollow section.

$$\varepsilon = \begin{cases} \sigma/E_s & (\sigma \le f_p) \\ \frac{\sigma}{E_s} + 0.002\left(\frac{\sigma}{\sigma_{0.2}}\right)^n & (f_p < \sigma \le \sigma_{0.2}) \\ \frac{\sigma-\sigma_{0.2}}{E_s} + \left[0.008 + \sigma_{1.0} - \sigma_{0.2}\left(\frac{1}{E_s} - \frac{1}{E_{0.2}}\right)\right] \left(\frac{\sigma-\sigma_{0.2}}{\sigma_{1.0}-\sigma_{0.2}}\right)^{n'_{0.2,1.0}} + \varepsilon_{0.2} & (\sigma_{0.2} < \sigma \le \sigma_{1.0}) \\ \frac{\sigma-\sigma_{1.0}}{k_2 E_s} + \varepsilon_{1.0} & (\sigma > \sigma_{1.0}) \end{cases} \quad (2)$$

where, ε is the strain of stainless steel;

σ is the stress of stainless steel;
E_s is the initial elastic modulus of stainless steel;
f_p is the proportional yield strength of stainless steel, and $f_p = k_1\sigma_{0.2}$;
$\sigma_{0.2}$ is the yield strength in accordance to 0.2% plastic strain;
$E_{0.2}$ is the tangent modulus corresponding to yield strength of $\sigma_{0.2}$, $\frac{E_{0.2}}{E_s} = \frac{1}{1+0.002n/e}$;
n is the strain hardening index, $n = \frac{\ln(20)}{\ln(\sigma_{0.2}/\sigma_{0.01})}$;
e is the coefficient, $e = \frac{\sigma_{0.2}}{E_s}$;
$n'_{0.2,1.0}$ is also a strain hardening index, $n'_{0.2,1.0} = 12.255\left(\frac{E_{0.2}}{E_s}\right)\left(\frac{\sigma_{1.0}}{\sigma_{0.2}}\right)+1.037$;

Based on regression of tested results of stainless steel coupons in this paper, k_1 is taken as 0.35, k_2 is taken as 0.02;

$\sigma_{1.0}$ is calculated according to $\sigma_{1.0}/\sigma_{0.2}=0.542/n+1.0$.
$\sigma_{0.01}$ is the stress in accordance to 0.01% plastic strain, and $\sigma_{0.01} = \varepsilon_{0.01}E_s$;

The stress analysis method from reference [34] is used in this paper. Different from CFSST, for SSTCC columns, the stainless steel tube would confine the lateral expansion of core concrete. In reality, the stress in radial direction of stainless steel tube is very small, which can be neglected. Thus, the stainless steel tube is assumed to be under the state of hoop tensile stress combining with axial compressive stress. According to the lateral and longitudinal strain of the stainless steel tube obtained from the tests, the axial stress σ_v, hoop stress σ_h and equivalent stress σ_z. on the stainless steel tube can be calculated based on the assumptions that:

- the stress in the radial direction of the tube is ignored;
- thin plate theory is used for the tube, therefore, the hoop stress is presumed evenly distributed along the thickness of the wall;
- the concrete core is under the axial and radius stress states;
- no slips are presumed between the tube and the concrete core.

The stress–strain relationships of stainless steel for each stage is as follows:

1) In the elastic stage, the stainless steel follows the Hooke's Law:

$$\begin{bmatrix} \sigma_h \\ \sigma_v \end{bmatrix} = \frac{E_0}{1-\mu_s^2}\begin{bmatrix} 1 & \mu_s \\ \mu_s & 1 \end{bmatrix}\begin{bmatrix} \varepsilon_h \\ \varepsilon_v \end{bmatrix} \quad (3)$$

where, μ_s is the Poisson's ratio for stainless steel.

2) In the plastic stage, the stainless steel follows Elastic–Plastic theory:

$$\begin{bmatrix} \sigma_h \\ \sigma_v \end{bmatrix} = \frac{E_s^t}{1-\mu_{sp}^2}\begin{bmatrix} 1 & \mu_{sp} \\ \mu_{sp} & 1 \end{bmatrix}\begin{bmatrix} \varepsilon_h \\ \varepsilon_v \end{bmatrix} \quad (4)$$

where, E_s^t is the secant modulus.

$$\frac{1}{E_s^t} = \begin{cases} \frac{1}{E_0} + \frac{0.002n\left(\frac{\sigma}{\sigma_{0.2}}\right)^{n-1}}{\sigma_{0.2}} & f_p \le \sigma < \sigma_{0.2} \\ \frac{1}{E_{0.2}} + \frac{\left[0.008 + (\sigma_{1.0}-\sigma_{0.2})\left(\frac{1}{E_0} - \frac{1}{E_{0.2}}\right)\right] n'_{0.2,1.0}\left(\frac{\sigma-\sigma_{0.2}}{\sigma_{1.0}-\sigma_{0.2}}\right)^{n-1}}{\sigma_{1.0}-\sigma_{0.2}} & \sigma_{0.2} \le \sigma \le \sigma_{1.0} \end{cases} \quad (5)$$

μ_{sp} is the Poisson's ratio of stainless steel in the plastic stage,

$$\mu_{sp} = 0.167\frac{\sigma - f_p}{f_y - f_p} + 0.283 \quad (6)$$

3) In the strain hardening stage

$$\begin{bmatrix} \sigma_h \\ \sigma_v \end{bmatrix} = \frac{E_s}{Q}\begin{bmatrix} \sigma_v'^2 + 2p & -\sigma_v'\sigma_h' + 2\mu_s p \\ -\sigma_v'\sigma_h' + 2\mu_s p & \sigma_h'^2 + 2p \end{bmatrix}\begin{bmatrix} \varepsilon_h \\ \varepsilon_v \end{bmatrix} \quad (7)$$

where, σ_v' is the axial stress, $\sigma_v' = \sigma_v - \sigma_{cp}$;

σ_h' is the hoop stress, $\sigma_h' = \sigma_h - \sigma_{cp}$;
σ_{cp} is the average stress, $\sigma_{cp} = (\sigma_h + \sigma_v)/3$;

$$p = \frac{2H'}{9E_s}\sigma_z^2 \quad (8)$$

$$H' = \frac{d\sigma}{d\varepsilon_p} = 10^{-3}E_s^2 \quad (9)$$

σ_z is the equivalent stress, $\sigma_z = \sqrt{\sigma_h^2 + \sigma_h^2 - \sigma_h\sigma_v}$;

$$Q = \sigma_h^2 + \sigma_v^2 + 2\mu_s\sigma_h\sigma_v + \frac{2H'(1-\mu_s)\sigma_z^2}{9G};$$

When the stresses such as σ_v, σ_h and σ_z are calculated, the axial force of the tube and the concrete core can be calculated correspondingly.

The axial force resisted by the stainless steel tube N_s:

$$N_s = \sigma_v A_s \quad (10)$$

where, A_s is the cross-sectional area of the tube; σ_v is the axial stress of the tube.

The axial stress of the concrete σ_c can also be derived as

$$\sigma_c = (N - N_s)/A_c \quad (11)$$

where, N is the axial load of the specimen; A_c is the cross-sectional area of core concrete.

4.1.2. Interaction behavior of stainless steel tube and core concrete for SSTCCs

Based on the above calculation method, the vertical stress and horizontal stress on the stainless steel tube for SSTCC members can be calculated. Fig. 9 shows the average stress–strain curves at the mid-height of the specimen. In Fig. 9(a), the symbol σ_v denotes the axial average stress, the symbol σ_h denotes the hoop stress, and the σ_z denotes the equivalent stress. For comparison of the values, the axial stress σ_v (compressive stress) defines as positive values. In the elastic stage, the axial stress σ_v increased with the increase of axial strain, and the hoop stress σ_h is nearly about zero. The axial stress is resulted from the friction between steel tube and core concrete. Thus, the steel tube at the mid-height of the specimen would resist the axial load. In this stage, the circumference deformation of concrete is very small and the interaction behavior between stainless steel tube and concrete is not obvious. When the axial strain ε_v reached 850 με, the corresponding stress of core concrete was equal to 39.4 MPa. At this point, the average stress of core concrete reached the compressive strength of concrete. Beyond this point, the hoop stress increased sharply with the increase of axial strain. When the equivalent stress reached the yield strength of $\sigma_{0.2}$, the corresponding axial stress and hoop stress are 309 MPa and 265 MPa, respectively. Under different strain level, the load resisted by the steel tube can be calculated, and then the load resisted by the core concrete can be calculated by subtracting the load resisted by stainless steel tube from the total axial load. Fig. 9(b) shows the average axial stress–strain curve of core concrete. It can be seen that when the steel tube reached its yield strength, the average compressive stress of core concrete reached 81 MPa, which is much higher than the maximum compressive stress of 54.5 MPa of unconfined concrete. This is due to the tube confinement to the core concrete. After the yielding of stainless steel tube, the hoop stress and equivalent stress could still increase as shown in Fig. 9(a) due to the significant strain hardening of stainless steel, which provide more confinement to core concrete and increase the average compressive stress of core concrete to 87 MPa.

4.1.3. Interaction behavior of stainless steel tube and core concrete for CFSSTs

The axial stress–strain curves on the stainless steel tube of concrete-filled stainless steel tubes are shown in Fig. 10(a). It can be seen that the axial stress of steel is almost same to the equivalent stress when the axial strain of steel is less than 3000 με. In addition, the hoop stress of steel is a negative value, which means the steel tube is under compression along the circumference direction. The reason was that the Poisson's ratio of concrete is smaller than that of steel. The radial deformation of steel is larger than that of concrete. However, the cohesion between steel and concrete restrained the radius deformation of steel tube. Thus, the hoop stress of steel tube appeared as compressive stress. With the increase of axial strain, the Poisson's ratio of concrete became larger than that of steel. The expansion deformation of core concrete became larger than that of steel. The stainless steel tube would confine the deformation of core concrete. When the equivalent stress reached the yield strength of stainless steel, the hoop stress on the steel tube is 50 MPa. The core concrete is under the state of three-directional compression. The compressive stress of core concrete reached 75 MPa, which is higher than that of concrete without confinement. Besides, the compressive stress of core concrete in CFSST columns is smaller than that in SSTCC columns, indicating that the confinement of stainless steel tube in CFSST columns is smaller than that in SSTCC columns.

4.2. Axial load-strain relationship curves

Figs. 11 and 12 show the axial load-strain curves of SSTCC and CFSST stub columns. For SSTCC stub columns, the axial strain is defined as the axial deformation divided by the height of the specimen. It can be seen that the rigidity and load-carrying capacity of each group of specimens with the same parameters are close to each other. The deformation ability of CFSST stub columns is better than that of SSTCC stub columns. The reason was that the hoop stress of SSTCC stub columns is larger than that of CFSST columns. The failure of the welding on SSTCC stub columns resulted in the premature failure of the specimens. Hence, for SSTCC columns, the hot-rolled stainless steel tubes are recommended in the construction.

4.3. Comparison of experimental results

Fig. 13 shows the comparison of SSTCC columns and CFSST columns with the same diameter. For SSTCC columns, the core concrete is subjected to compression and the stainless steel tube would not contribute to resisting the vertical load directly. While for CFSST columns, the steel tube and core concrete are loaded simultaneously. From Fig. 13, it can be seen that the load-carrying capacity of SSTCC columns is higher than that of CFSST columns. For specimens with diameter-to-thickness ratios of 108, 97 and 90, the increase ratios of load-carrying capacity are 2.5%, 6.4% and 7.5%, respectively.

The rigidity of stainless steel tube confined concrete member is obviously lower than that of concrete-filled steel tubes. The rigidity of steel tube confined concrete member decreases about 20%. In addition, the deformation corresponding to peak load of SSTCC column is larger

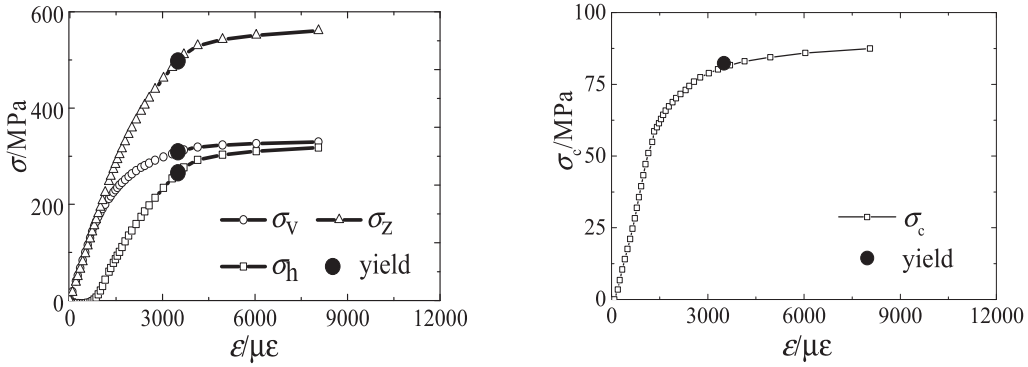

(a) Axial stress vs. strain on stainless steel tube (b) Axial stress vs. strain of the core concrete

Fig. 9. Average stress and strain relationship curves of specimen SSTCC-D125-a.

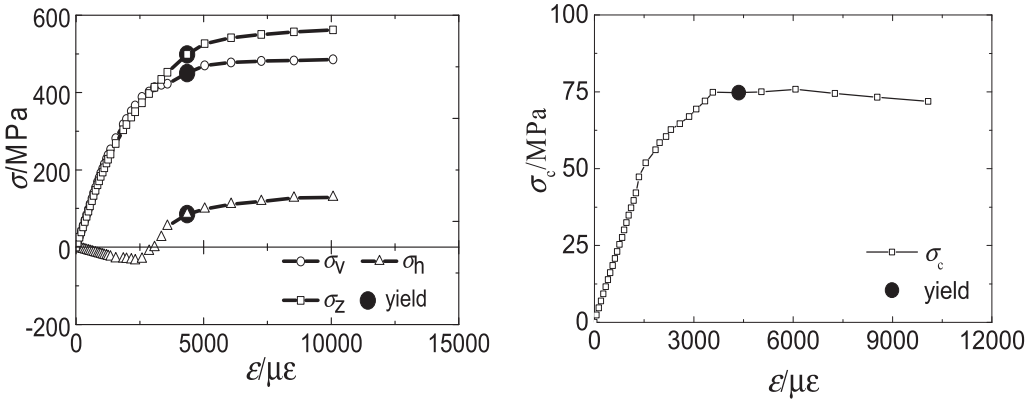

(a) Axial stress vs. stain of steel tube (b) Axial stress vs. stain of core concrete

Fig. 10. Average stress and strain relationship curves of specimen CFSST-D150-1.

than that of CFSST column. For steel tube confined concrete member, in the elastic stage, the steel tube has little contribution to the rigidity. While for CFSST columns, the steel tube would resist part of the vertical load in the elastic stage. In the elastic-plastic stage, the hoop stress of tube increases which would decrease the axial compressive stress of steel tube according to Von-Mises criterion.

5. Axial strength of stainless steel tube confined stub columns

Although the stainless steel tube in SSTCC column is not supposed to contribute to the axial compressive resistance, based on the experimental results, it was found that the stainless steel tube at the mid-height would still resist part of the axial load even the stainless steel tube is cut on both ends. This is due to the friction between steel tube and core concrete, which enable the steel tube to resist the axial load. The hoop stress on the steel tube would confine the concrete, thus the concrete was under the state of three-directional compression. The compressive strength of confined concrete was proposed by Mander et al. [35]:

$$f_{cc} = f_c'\left(-1.245 + 2.245\sqrt{1 + 7.94\frac{f_r'}{f_{co}}} - 2\frac{f_r'}{f_{co}}\right) \tag{12}$$

where, f_r' is the effective confining stress of circular tube on the concrete, which can be calculated as follows:

$$f_r' = \frac{2t\sigma_h}{D - 2t} \tag{13}$$

The stainless steel is also assumed to obey the Von-Mises yielding criterion as follows:

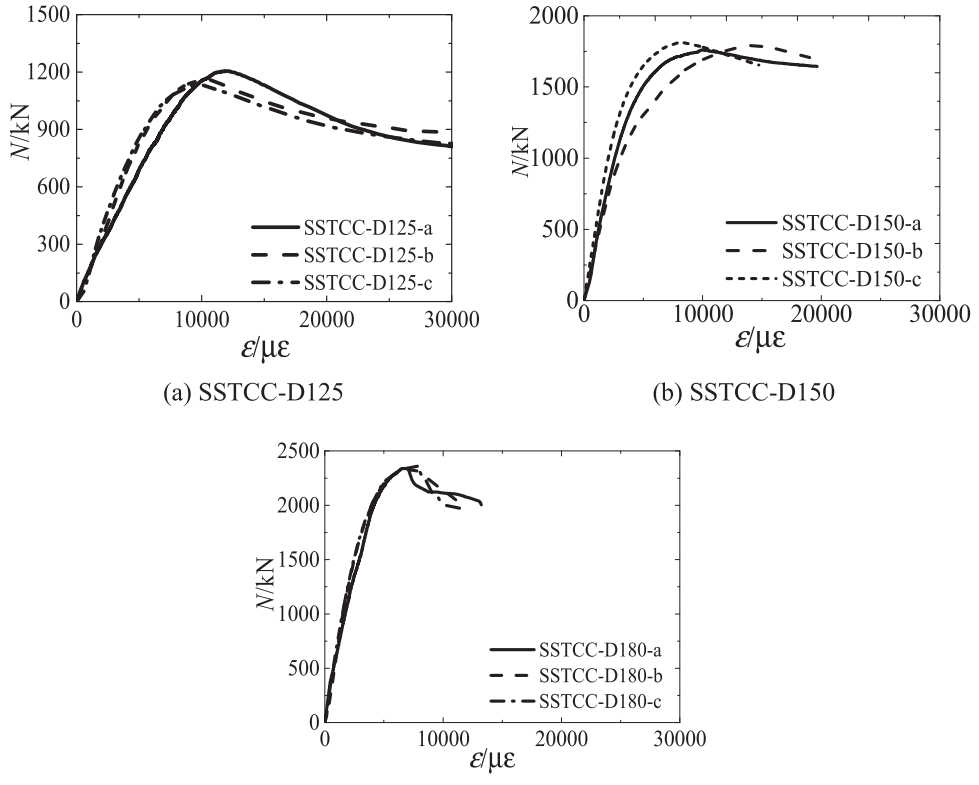

(a) SSTCC-D125 (b) SSTCC-D150

(c) SSTCC-D180

Fig. 11. Axial strain vs. axial load relationship of SSTCC stub columns.

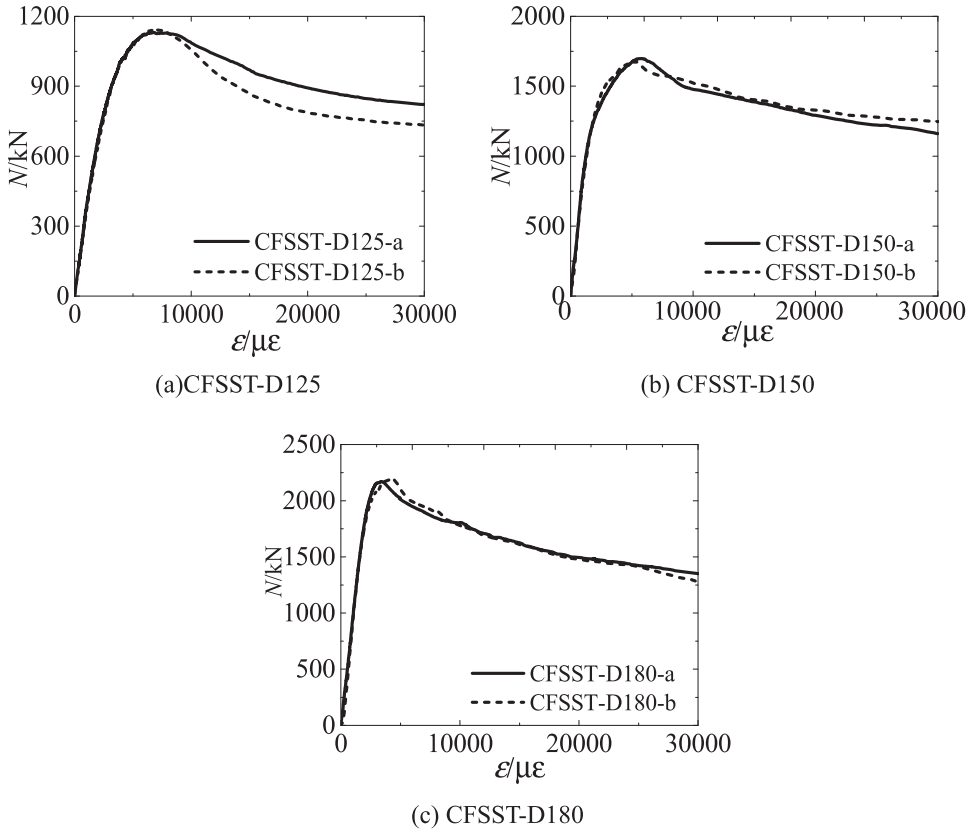

(a)CFSST-D125 (b) CFSST-D150

(c) CFSST-D180

Fig. 12. Axial strain and load relationship of CFSST stub columns.

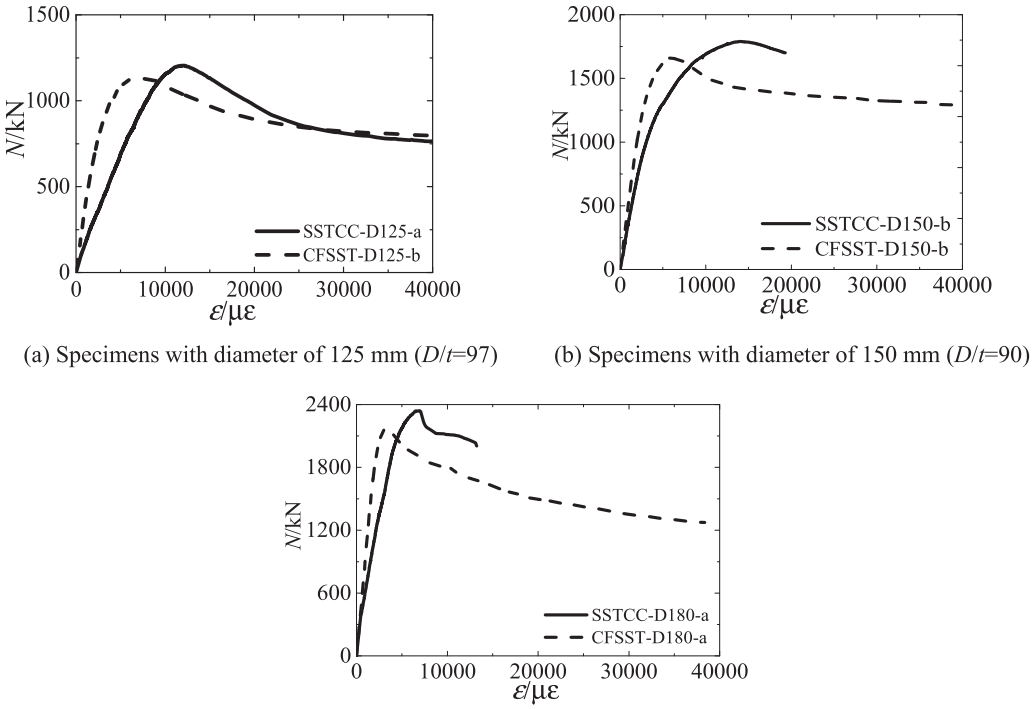

(a) Specimens with diameter of 125 mm (D/t=97) (b) Specimens with diameter of 150 mm (D/t=90)

(c) Specimens with diameter of 180 mm (D/t=108)

Fig. 13. Comparison between SSTCC and CFSST.

$$\sigma_z = \sqrt{\sigma_h^2 + \sigma_v^2 - \sigma_h \sigma_v} \quad \text{and} \quad \sigma_z \le \sigma_{0.2} \qquad \sigma_{0.2} = \sqrt{\sigma_h^2 + \sigma_v^2 - \sigma_h \sigma_v} \tag{14}$$

When the stainless steel reached the yield strength, it can be assumed that the steel meets the following equation.

After the axial stress σ_v is known, the corresponding hoop stress σ_h can be calculated according to Eq. (14).

Table 2
Comparison between test results and calculated results.

No.	*D/mm*	*t/mm*	Δ_u/mm	N_{s+c}/kN	N_{ue}/kN	N_c/kN	N_c/N_{ue}	N_{ue}/N_{s+c}
SSTCC-D125-a	125.3	1.29	3.59	905	1205	1174	0.974	1.33
SSTCC-D125-b	124.8	1.25	3.61	905	1160	1153	0.994	1.28
SSTCC-D125-c	124.5	1.33	3.63	905	1131	1175	1.039	1.25
CFSST-D125-a	124.8	1.31	2.72	905	1131	1047	0.926	1.25
CFSST-D125-b	125.3	1.3	2.72	905	1142	1051	0.920	1.26
SSTCC-D150-a	149.7	1.63	4.67	1305	1759	1650	0.938	1.35
SSTCC-D150-b	149.8	1.67	6.43	1305	1790	1666	0.931	1.37
SSTCC-D150-c	150.2	1.67	3.86	1305	1812	1674	0.924	1.39
CFSST-D150-a	150.1	1.68	2.81	1305	1698	1544	0.910	1.30
CFSST-D150-b	149.8	1.65	2.83	1305	1661	1530	0.921	1.27
SSTCC-D180-a	180.8	1.68	4.14	1730	2340	2275	0.972	1.35
SSTCC-D180-b	180.6	1.65	3.94	1730	2333	2257	0.968	1.35
SSTCC-D180-c	180.7	1.67	4.25	1730	2360	2269	0.961	1.36
CFSST-D180-a	180.7	1.69	2.08	1730	2169	2109	0.972	1.25
CFSST-D180-b	180.7	1.7	2.25	1730	2193	2113	0.963	1.27

Note: Δ_u is the displacement corresponding to the load-carrying capacity; N_{ue} is the capacity of experimental results; N_{s+c} is the sum capacity of steel and concrete; N_c is the calculated capacity of specimen.

Based on the test results of SSTCC columns, it was found that when the specimens reached their load-carrying capacity, the axial stress on the steel tube is about 60% of yield strength. According to the Von-Mises criterion, the hoop stress on the steel tube is 0.55 times of yield strength. Based on the test results of CFSST columns, it was found that the axial stress on the steel tube is about 0.9 times of yield strength of steel when the specimens reached their load-carrying capacity, and the corresponding hoop stress on the steel tube is 0.18 times of yield strength. Thus, the following equation is suggested to calculate the loading-carrying capacity of stainless steel tube confined concrete stub columns and concrete-filled stainless steel tube stub columns.

$$N_u = f_{cc}A_c + A_s\sigma_v \tag{15}$$

$$\sigma_v = \beta\sigma_{0.2} \tag{16}$$

$$\sigma_h = \frac{\sqrt{4-3\beta^2}-\beta}{2}\sigma_{0.2} \tag{17}$$

in which, β is the proportional factor of axial stress corresponding to the yield strength of steel; f_{cc} can be calculated by Eq. (12). A_c is the area of core concrete; A_s is the area of steel tube. As analyzed above, the factor β is 0.6 for SSTCC columns while 0.9 for CFSST columns. Using the Eq. (15), the load-carrying capacities of all specimens are calculated and listed in Table 2. It can be seen that the calculated results are close to the experimental results, indicating that the proposed equation can be used to calculate the load-carrying capacity of stainless steel tube confined concrete columns and concrete-filled stainless steel tubes columns. In addition, the sum of concrete and stainless steel tube capacities are listed in Table 2. It can be seen that the capacities of SSTCC columns are about 34% higher in average than the sum of concrete and steel tube, while the capacities of CFSST columns are about 27% higher in average than the sum of concrete and steel tube. The reason is that the core concrete is confined by a stainless steel tube in all columns and the confinement of stainless steel tube in SSTCC columns is larger than that in CFSST columns.

6. Conclusions

This paper studied the behavior of axially loaded stainless steel tube confined concrete stub columns and concrete-filled stainless steel tube stub columns. The experimental phenomena were introduced in detail and the interaction between stainless steel tube and core concrete was studied based on the axial stress and hoop stress on the stainless steel tube. In addition, an equation was proposed to predict the axial strength of stainless steel tube confined concrete columns considering the contribution of confined concrete and stainless steel tube. In future study, the numerical analysis of stainless steel tube confined concrete columns should be performed to deeply understand the influence of steel yield strength, concrete strength, and steel ratio on the axial loaded and eccentric loaded behavior of this kind of specimens. Based on all the analysis, the following conclusions can be drawn:

(1) Both stainless steel tube confined concrete stub columns and concrete-filled stainless steel tube stub columns possess high load-carrying capacity. The load-carrying capacity of stainless steel tube confined concrete members is higher than that of concrete-filled stainless steel tube stub columns.
(2) The quality of welding is a key factor for steel tube confined specimens, which would influence the deformation ability of the specimens. The seamless steel tubes are suggested to be used for stainless steel tube confined concrete members.
(3) For stainless steel tube confined concrete members, although the stainless steel tube is cut on both ends, the steel tube would still resist a certain percentage of the overall vertical load. Based on the test results, the contribution of axial stress of steel tube to the load-carrying capacity should be considered.
(4) A formula to calculate the load-carrying capacity of stainless steel tube confined concrete members is proposed, which is also can be used to calculate the load-carrying capacity of concrete-filled stainless steel tube stub columns.

Acknowledgements

This research was financially supported by the National Natural Science Foundation of China (Grant no. 51778185), the Jilin Science and Technology Development Project (20180201031SF), and the Major (key) Projects of Key R & D Projects in the Ningxia Hui Autonomous Region (2018BEG02009). The authors wish to acknowledge the sponsors. However, any opinions, findings, conclusions and recommendations presented in this paper are those of the authors and do not necessarily reflect the views of the sponsors.

References

[1] J. Liu, S. Zhang, X. Zhang, et al., Behavior and strength of circular tube confined reinforced-concrete (CTRC) columns, J. Constr. Steel Res. 65 (7) (2009) 1447–1458.
[2] X. Wang, J. Liu, S. Zhang, Behavior of short circular tubed-reinforced-concrete columns subjected to eccentric compression, Eng. Struct. 105 (2015) 77–86.
[3] J. Liu, X. Zhou, Behavior and strength of tubed RC stub columns under axial compression, J. Constr. Steel Res. 66 (1) (2010) 28–36.
[4] P. McAteer, J.F. Bonacci, M. Lachemi, Composite response of high-strength concrete confined by circular steel tube, Struct. J. 101 (4) (2004) 466–474.
[5] H. Mei, P.D. Kiousis, M.R. Ehsani, et al., Confinement effects on high-strength concrete, Struct. J. 98 (4) (2001) 548–553.

[6] F. Liu, H. Yang, L. Gardner, Post-fire behaviour of eccentrically loaded reinforced concrete columns confined by circular steel tubes, J. Constr. Steel Res. 122 (2016) 495–510.
[7] J. Liu, Y. Teng, Y. Zhang, et al., Axial stress–strain behavior of high-strength concrete confined by circular thin-walled steel tubes, Constr. Build. Mater. 177 (2018) 366–377.
[8] F. Liu, L. Gardner, H. Yang, Post-fire behaviour of reinforced concrete stub columns confined by circular steel tubes, J. Constr. Steel Res. 102 (2014) 82–103.
[9] M. Nematzadeh, S. Fazli, M. Naghipour, et al., Experimental study on modulus of elasticity of steel tube-confined concrete stub columns with active and passive confinement, Eng. Struct. 130 (2017) 142–153.
[10] A. Le Hoang, E. Fehling, Numerical study of circular steel tube confined concrete (STCC) stub columns, J. Constr. Steel Res. 136 (2017) 238–255.
[11] Y.H. Wang, W. Wang, J. Chen, Seismic behavior of steel tube confined RC columns under compression-bending-torsion combined load, J. Constr. Steel Res. 143 (2018) 83–96.
[12] X. Wang, J. Liu, X. Zhou, Behaviour and design method of short square tubed-steel-reinforced-concrete columns under eccentric loading, J. Constr. Steel Res. 116 (2016) 193–203.
[13] J. Liu, X. Wang, S. Zhang, Behavior of square tubed reinforced-concrete short columns subjected to eccentric compression, Thin-Walled Struct. 91 (2015) 108–115.
[14] X. Zhou, B. Yan, J. Liu, Behavior of square tubed steel reinforced-concrete (SRC) columns under eccentric compression, Thin-Walled Struct. 91 (2015) 129–138.
[15] B. Young, E. Ellobody, Experimental investigation of concrete-filled cold-formed high strength stainless steel tube columns, J. Constr. Steel Res. 62 (5) (2006) 484–492.
[16] E. Ellobody, Nonlinear behavior of concrete-filled stainless steel stiffened slender tube columns, Thin-Walled Struct. 45 (3) (2007) 259–273.
[17] E. Ellobody, B. Young, Design and behaviour of concrete-filled cold-formed stainless steel tube columns, Eng. Struct. 28 (5) (2006) 716–728.
[18] D. Lam, L. Gardner, Structural design of stainless steel concrete filled columns, J. Constr. Steel Res. 64 (11) (2008) 1275–1282.
[19] M.F. Hassanein, O.F. Kharoob, Q.Q. Liang, Circular concrete-filled double skin tubular short columns with external stainless steel tubes under axial compression, Thin-Walled Struct. 73 (2013) 252–263.
[20] S. Abdalla, F. Abed, M. AlHamaydeh, Behavior of CFSTs and CCFSTs under quasi-static axial compression, J. Constr. Steel Res. 90 (2013) 235–244.
[21] Y. Ye, S.J. Zhang, L.H. Han, et al., Square concrete-filled stainless steel/carbon steel bimetallic tubular stub columns under axial compression, J. Constr. Steel Res. 146 (2018) 49–62.
[22] L.H. Han, Q.X. Ren, W. Li, Tests on stub stainless steel–concrete–carbon steel double-skin tubular (DST) columns, J. Constr. Steel Res. 67 (3) (2011) 437–452.
[23] F. Wang, L. Han, W. Li, Analytical behavior of CFDST stub columns with external stainless steel tubes under axial compression, Thin-Walled Struct. 127 (2018) 756–768.
[24] R. Feng, Y. Chen, J. Wei, et al., Experimental and numerical investigations on flexural behaviour of CFRP reinforced concrete-filled stainless steel CHS tubes, Eng. Struct. 156 (2018) 305–321.
[25] Y. Chen, R. Feng, Y. Shao, et al., Bond-slip behaviour of concrete-filled stainless steel circular hollow section tubes, J. Constr. Steel Res. 130 (2017) 248–263.
[26] Y. Chen, K. Wang, R. Feng, et al., Flexural behaviour of concrete-filled stainless steel CHS subjected to static loading, J. Constr. Steel Res. 139 (2017) 30–43.
[27] Y. Chen, R. Feng, L. Wang, Flexural behaviour of concrete-filled stainless steel SHS and RHS tubes, Eng. Struct. 134 (2017) 159–171.
[28] Y.L. Li, X.L. Zhao, R.K.R. Singh, et al., Tests on seawater and sea sand concrete-filled CFRP, BFRP and stainless steel tubular stub columns, Thin-Walled Struct. 108 (2016) 163–184.
[29] V.I. Patel, Q.Q. Liang, M.N.S. Hadi, Nonlinear analysis of axially loaded circular concrete-filled stainless steel tubular short columns, J. Constr. Steel Res. 101 (2014) 9–18.
[30] M. Dabaon, S. El-Khoriby, M. El-Boghdadi, et al., Confinement effect of stiffened and unstiffened concrete-filled stainless steel tubular stub columns, J. Constr. Steel Res. 65 (8–9) (2009) 1846–1854.
[31] GB/T 228-2002, Metallic Materials-Tensile Testing at Ambient Temperature. Beijing, China, 2002.
[32] GB/T 50081-2002, Standard for Test Method of Mechanical Properties on Ordinary Concrete. Beijing, China, 2002.
[33] W.M. Quach, J.G. Teng, K.F. Chung, Three-stage full-range stress–strain model for stainless steels, J. Struct. Eng. 134 (9) (2008) 1518–1527.
[34] S. Zhang, L. Guo, Z. Ye, et al., Behavior of steel tube and confined high strength concrete for concrete-filled RHS tubes, Adv. Struct. Eng. 8 (2) (2005) 101–116.
[35] J.B. Mander, M.J.N. Priestley, R. Park, Theoretical stress–strain model for confined concrete, J. Struct. Eng. 114 (8) (1988) 1804–1826.